Revue de Métallurgie **109**, 5–10 (2012)
© EDP Sciences, 2012
DOI: 10.1051/metal/2011074
www.revue-metallurgie.org

Revue de Métallurgie

Spark plasma sintering for metallic glasses processing

L. Perrière, M.-T. Thaï, S. Tusseau-Nenez, P. Ochin, M. Blétry and Y. Champion

ICMPE, CNRS UMR 7182, 2-8 rue Henri Dunant, 94320 Thiais, France
e-mail: champion@icmpe.cnrs.fr

Key words:
Metallic glass; zirconium; spark plasma sintering; mechanism

Received 16 November 2011
Accepted 18 November 2011

Abstract – Development of metallic glasses is hindered by the difficulties in manufacturing bulk parts. We report on the preparation of glassy alloys using the spark plasma sintering of gas atomized powders. The $Zr_{57}Cu_{20}Al_{10}Ni_8Ti_5$ alloy processed has a high glass forming ability. Densification is obtained at the glass transition temperature (390 °C) under high pressure (≈500 MPa). Systematic study of the effect of powder particles size and sintering time is performed through structural and thermal analyses. Local and partial devitrification of the amorphous alloy is detected, resulting from local temperature overshoots. From these analyses, an approach of the spark plasma sintering mechanism of metallic glasses is proposed.

Bulk metallic glasses (BMGs) elaboration has been developed since the 1960s. Formation of amorphous alloys is kinetically controlled and obeys empirical rules stated by Inoue [1]. BMGs are essentially manufactured using casting and rapid quenching techniques, limiting dimensions and shapes of the available pieces [2]. One interesting way consists in preparing bulk pieces from a fine amorphous powder (even presenting a low glass forming ability) [3]. In this respect, atomization of MG powders has been studied since the early 1980s [4]. Attempts for sintering were carried out by hot pressing [5], extrusion [6] and, more recently, by spark plasma sintering [7–13].

This paper deals with the analysis of SPS densification of a $Zr_{57}Cu_{20}Al_{10}Ni_8Ti_5$ MG prepared by gas atomization. Several studies have already been performed on this alloy, and is thus the relevant reference for comparison with sintered parts [14, 15]. Structural and thermal analyses of sintered samples with various grain sizes have been carried out in order to identify specific SPS densification and consolidation mechanisms. This study aims at approaching the specific mechanisms of SPS of MGs, with particular interest in localized phenomena (in particular at particles sintering necks).

1 Experimental

Powders prepared by high pressure gas atomization [16] were sintered in a Syntex SPS-515S (Syntex, Japan), using WC/Co die and punches. For $Zr_{57}Cu_{20}Al_{10}Ni_8Ti_5$, the sintering and densification temperature domain available is narrow (about 60 °C) between the glass transition temperature ($T_g \approx 385$ °C) and the crystallisation temperature ($T_x \approx 450$ °C). For our experiments, the temperature of the sintering plateau has thus been fixed at 390 °C (just above T_g). To reach full densification, samples (10 mm in diameter and 4.5 mm final thickness) were compressed at a loading rate of 20 kN.min^{-1} up to 40 kN (about 500 MPa on the sample). A heating rate of 60 °C.min^{-1} was then applied from room temperature up to 300 °C. The heating rate was slowed down to 10 °C.min^{-1} from 300 °C to 390 °C. Holding time varied from 3 to 10 min, depending on the sample (see Tab. 1 for experimental details). All experiments were carried out under vacuum (7.5×10^2 torr). The necessary electric energy for heating is provided by high current intensity (intensity is recorded up to ≈1200–1300 A), balanced by an appropriate voltage (less than 2V). In the Syntex equipment, the pulsed current is periodically input following a set of

https://doi.org/10.1051/metal/2011074 Published online by Cambridge University Press
Article published by EDP Sciences

Table 1. Experimental details, values of density, enthalpy of first crystallization measured by DSC and failure stress (measured in compression, at $\dot{\epsilon} = 5 \times 10^{-5}$ s^{-1}), compared to a bulk sample prepared by casting.

Sample	holding time (min)	Powder grain size (μm)	Density	H_{crys} (J.g^{-1})	σ_{max} (MPa)
bulk	–	–	6.59	61.9	1700
G1	3	No selection: $d_{50} = 70$	6.57	36.8	1250
G2	5	No selection: $d_{50} = 70$	6.59	23.7	1300
G3	5	32–63	6.60	43.5	1625
G4	5	63–125	6.58	51.0	1400
G5	10	32–63	6.61	37.4	1675
G6	10	63–125	6.60	45.2	1650

12 pulses (2 ms on 1 ms off) followed by 2 pauses (3 ms off). Temperature is monitored through a K-type thermocouple inserted in the die at approximately 2.5 mm of the sample. Density measurements were performed using Archimedes principle, using propan-1-ol as a medium. Thermal analysis was performed using differential scanning calorimetry (DSC Mettler-Toledo DSC822 calorimeter, Intl. Inc., Switzerland) at a heating rate of 20 °C.min^{-1}. Structural characterisation was carried out by XRD measurements, with a X-ray powder diffractometer (XPert PRO MPD, PANalytical, the Netherlands). Local observations were performed with an analytical transmission electron microscope (TEM TECNAI-FEI F20, FEI, USA) operating at 200 kV. The thin foils were prepared by mechanical polishing and Ar^+ ion beam milling. Finally, mechanical behavior was assessed by uni-axial compressive experiments, carried out on a 100 kN MTS-20/M system, at a strain rate of 5×10^{-5} s^{-1}.

2 Results

Efficiency of SPS for sintering MG powders was studied with respect to annealing time and particles size, which are detailed in Table 1. From DSC measurements plotted in Figure 1, one can first notice that the enthalpy of first crystallization for all the sintered samples (G1 to G6) is lower than the one measured on the bulk, as well as on the powder (54.8 J.g^{-1} [16]), indicating that partial devitrification is likely occuring during the SPS annealing. Moreover, comparison of values measured on G2, G3 and G4 (see Fig. 1) indicates that devitrification is linked to the particles size. Indeed,

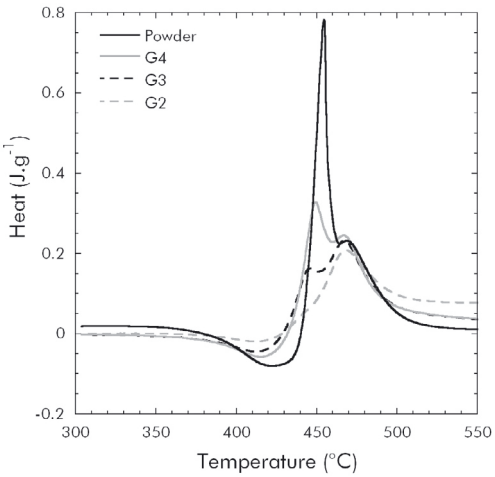


Fig. 1. DSC scans of $Zr_{57}Cu_{20}Al_{10}Ni_8Ti_5$ amorphous powder and G2-G4 sintered samples.

small particle size and wide particle size distributions result in an increased average number of contacts points between particles, and consequently in a larger devitrification amount. Finally, from Table 1, it also comes that $H_{G4} > H_{G6}$, $H_{G2} > H_{G1}$ and $H_{G3} > H_{G5}$, meaning that G1, G5 and G6 are more crystallized than G2, G3 and G4, respectively. According to this, increasing annealing time logically induces more crystallization in the sample.

Occurence of partial crystallization is supported by TEM observations, as shown in Figure 2. Crystalline particles with diameter of about 20 nm are visible on the polygonal surfaces, which correspond to former neck zones between particles.

Partial X-ray diffraction patterns for G2 and G5 are displayed in Figure 3. XRD confirms the partial devitrification of MG during SPS, as already observed on DSC experiments (see Tab. 1 for enthalpy values).

https://doi.org/10.1051/metal/2011074 Published online by Cambridge University Press

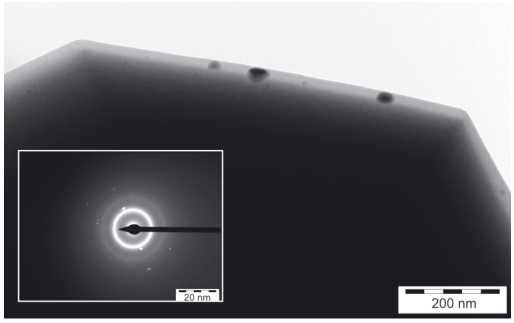


Fig. 2. TEM micrograph of a sintered sample, where nano-precipitates are clearly present in the central part of the particle facet. Inset: selected area diffraction pattern showing broad rings characterizing the amorphous matter, but also some crystalline spots.

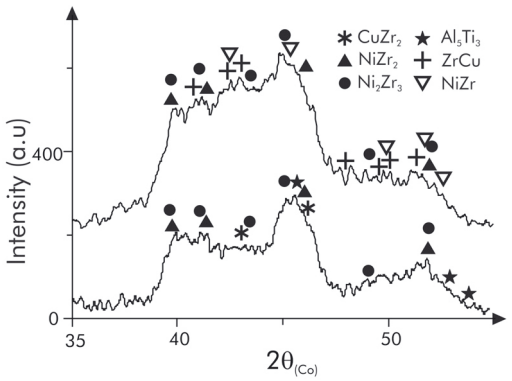


Fig. 3. Zoom on small angles of XRD patterns obtained on G2 and G5, with indexed crystallized phases.

Indeed, for sintered samples, crystaline reflections appear superimposed the broad peaks of the amorphous phase. For G5, the main phase produced during SPS is Ni_2Zr_3 (which is metastable), in equilibrium with $NiZr_2$, NiZr and ZrCu. For G2, Al_5Ti_3, Ni_2Zr_3, $NiZr_2$ and $CuZr_2$ have been identified. One can notice that no reflection of any oxide, especially ZrO_2, has been detected in any sample. The ZrCu phase, wich is stable above 730 °C according to the phase diagrams, has also been detected on G3 and G4 (short annealing time, see Tab. 1). It indicates that high temperature and less stable phases (as ZrCu or Ni_2Zr_3) appear first at short annealing time and likely react with the amorphous matrix after further annealing to form stable phases at room temperature; like $CuZr_2$ or $NiZr_2$.

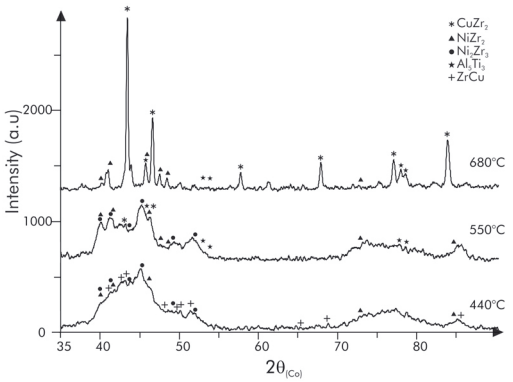


Fig. 4. XRD patterns obtained on annealed bulk samples of $Zr_{57}Cu_{20}Al_{10}Ni_8Ti_5$ MG. Temperatures of annealing are 440, 550 and 680 °C. Heating rate was fixed at 10 °C.min^{-1}.

Moreover, XRD analyses were carried out on annealed samples at 440, 550 and 680 °C, which correspond to the peaks of crystallization of the alloy, as shown in Figure 4. At 440 °C, the amorphous phase related broad bands are still present, but presence of some crystalline reflections, corresponding to ZrCu and Ni_2Zr_3 metastable phases, can be noticed. Those two phases appear first during the devitrification process of the alloy, likely because their atomic arrangement is the closest of the amorphous atomic stacking. At 550 °C, further crystallization is observed, even if some amorphous phase seems to be still present. New phases are detected, such as Al_5Ti_3, or $CuZr_2$, which is stable at room temperature and probably appears by reaction of ZrCu (no longer visible at 550 °C) and the amorphous matrix. Finally, at 680 °C, the amorphous alloy seems to be fully crystallized, as no amorphous signal has been detected. Furthermore, no reflections from metastable phases are detected.

Results indicate that full densification (see values of density listed in Tab. 1) of MGs using SPS (with pulsed current), is reached through two distinct steps. The cohesion between particles is first achieved during initial stages of the sintering at the contact between powder particles. This first step occurs at narrow necks (meaning the current density at the necks is large, thus leading to large increase of temperature), but leads to partial cohesion, along with partial

https://doi.org/10.1051/metal/2011074 Published online by Cambridge University Press

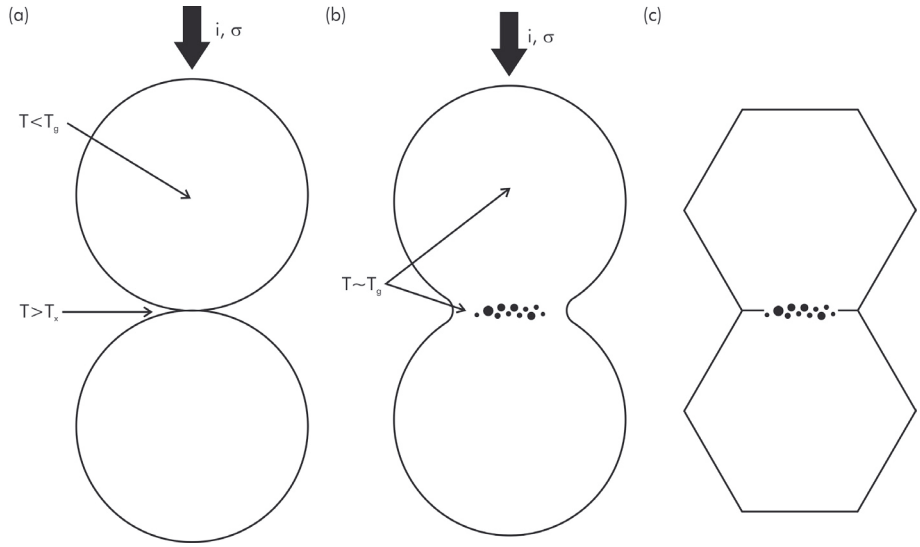


Fig. 5. Schematic representation of the compaction mechanism of MG by SPS: (a) during the early stages, neck size is very fine, leading to high current densities in their vicinity, and thus likely to temperatures larger than T_x, responsible for nano precipitation in those areas; (b) when the neck size is sufficient, all the particle is homogeneously heated at around T_g, leading to plastic flow; (c) total densification is finally reached.

devitrification of the MG (Fig. 5a). However, as total densification is reached, further densification is then happening during a second stage of the sintering process. It is occurring when necks are wide enough to allow homogeneous heating of the powder particles at around T_g, thus allowing Newtonian flow of the MG but avoiding further crystallisation in the vicinity of necks (Fig. 5b). According to this study, those two steps are believed to lead to complete densification. However, this process is also responsible for the apparition of a minor devitrification localised in the vicinity of the particles contacts (Fig. 5c).

Those results, and especially the observation of nano-precipitates (Fig. 2), suggest that, in some parts of the sample, the temperature was large enough to allow precipitation and growth of crystalline particles through diffusion processes, as well as bonding powder particles. Moreover, identification of phases of the kind of ZrCu also suggests that during certain stages of the proces, temperature can be at least higher that T_x. However, one can emphasize that the MG is not fully devitrified (Fig. 3). Furthermore, ZrCu, a high temperature stable phase, is one of the first crystallized phase appearing (Fig. 4). It then follows that the balance between temperature increase (due to Joule effect) and thermal dissipation from the necks, leads to an average temperature not too much larger than T_x.

The balance between Joule effect (temperature rise at the necks) and heat flow (dissipation of the temperature gradient taking place between the necks and the centre of the powder particles) gives the local temperature rate as: $\Delta T/\Delta t \approx \left(\rho_e j^2\right) / \left(\rho_v C_p\right)$, where ρ_e is the electrical resistivity, ρ_v the volume weight and C_p the heat capacity. Considering six average contacts per powder particle (average number of contacts in spheres random packing), then one can predict the temperature rise in the vicinity of a neck according to: $\Delta T_{\text{neck}} \approx (\Delta T_{\text{core}}/9) / (R/x)^4$, where R stands for the radius of the particle and x for the radius of the neck. It naturally comes that the difference in temperatures between the particle core and the neck region varies as the sintering degree (x/R), and that the power of 4 means that, at small neck sizes (i.e. early stages of the sintering) this difference is substantial. The temperature gradient between the neck region and the particle core leads to heat dissipation from these two respective zones, with relaxation time of the order of $\tau \approx R^2/\alpha \approx 0.4$ ms, with the thermal

https://doi.org/10.1051/metal/2011074 Published online by Cambridge University Press

diffusivity, $\alpha = 3.5 \times 10^6$ m^2.s^{-1} [17]. τ is smaller than the on (2 ms) and off (1 ms) times of an elemental pulse, and is certainly overestimated. As a matter of fact, in this estimate, heat dissipation is supposed to occur only by conduction in a cylinder of radius x (radius of the neck), and a large quantity of matter off this virtual cylinder is not considered for dissipating energy. Nevertheless, this rough analysis of the thermal evolution by current heating, indicates that heat dissipation from the neck to the particle core occurs concomitantly to heat accumulation by Joule effect at the neck. Analytical evaluation of an effective temperature as a function of time at the neck region is thus not possible since those two concurrent effects have different time and spatial scales. This would most likely demand relevant numerical simulations.

Owing to rapid heat dissipation from neck to particle core, homogeneous temperature is rapidly obtained in the overall sample after the off (1 ms) time, which means that the monitoring of temperature by external recording is likely consistent. Most dramatic is the substantial increase of temperature in the neck region. For example, one may consider a spontaneous event that is heat accumulation by Joule effect with negligible dissipation: $\Delta t \ll \tau$. Taking $\Delta t \approx \tau/100$, the temperature rises higher than T_x (ΔT starting from room temperature) for neck sizes smaller than 500 nm during such a spontaneous event. This rough evaluation shows that, since the very beginning of the sintering, the SPS pulses are able to produce spontaneous temperature increases larger than T_x. The heat is most likely maintained to this range of temperature by cumulative events during the 12 pulses sequence, and then totally dissipated during the 6 ms extra-pauses sequence. These local temperature increases are obviously not detected by external average measurements, since the pulses frequency is very high and the total volume of the neck regions is very small, $\approx (x/R)^4/4$.

3 Conclusions

Spark plasma sintering was efficiently used to produce sintered $Zr_{57}Cu_{20}Al_{10}Ni_8Ti_5$ bulk metallic glass with strength similar to that of the bulk alloy produced by solidification. This process opens interesting perspectives for the production of multiphase and architectured materials having selected properties. Characterisation of the sintered parts using X ray diffraction, differential scanning calorimetry and transmission electron microscopy revealed elemental features of the micromechanisms involved in the sintering process of this particular metallic glass, but also leading to some extension to metallic powders more generally.

Densification of MGs using SPS might thus be described as follows: heat level generated at initial particles necks is extremely large in the first stage of the sintering, when necks are small, and its relaxation is very fast due to high thermal diffusivity of metallic alloys. High intensity pulsed current is thus detrimental, and leads to partial devitrification of the metallic glass, formation of high temperature phases and stress gradient by alternate heating and cooling. When necks are wide enough to limit current density, heating becomes homogeneous, and amorphous particles can flow, thus leading to a total densification. It must be emphasized that these first stages of sintering are dominant for the properties of the sintered MG. Unfortunately, those events cannot be controlled by macroscopic monitoring in SPS (temperature measurements and sintering rate) since they are localised in the vicinity of particle necks, and their volume fraction is negligible. Gradual increase of the macroscopic current intensity to moderate current density at the growing particles neck seems relevant to avoid detrimental temperature as well as pronounced devitrification. Finite elements modelling should be useful in order to control these localized processes.

References

[1] A. Inoue, *Acta Materialia* **48** (2000) 279-306
[2] A.L. Greer, *Mater. Today* **12** (2009) 14–22
[3] R. Orrù, R. Licheri, A.M. Locci, A. Cincotti, G. Cao, *Mater. Sci. Eng. R* **63** (2009) 127-287
[4] S.A. Miller, R.J. Murphy, *Scripta Metall.* **13** (1979) 673-676
[5] Y.B. Kim, H.M. Park, W.Y. Jeung, J.-S. Bae, *Mater. Sci. Eng. A* **368** (2004) 318-322

https://doi.org/10.1051/metal/2011074 Published online by Cambridge University Press

[6] D.J. Sordelet, E. Rozhkova, P. Huang, P.B. Wheelcock, M.F. Besser, M.J. Kramer, M. Calvo-Dahlborg, U. Dahlborg, *J. Mater. Res.* **17** (2002) 186-198
[7] T.-S. Kim, J.-K. Lee, H.-J. Kim, J.-C. Bae, *Mater. Sci. Eng. A* **402** (2005) 228-233
[8] G. Xie, W. Zhang, D.V. Louzguine-Luzgin, H. Kimura, *Scripta Materialia* **55** (2006) 687-690
[9] J.K. Lee, H.J. Kim, T.S. Kim, Y.C. Kim, J.C. Bae, *J. Alloys Compd.* **434-435** (2007) 336-339
[10] G. Xie, D.V. Louzguine-Luzgin, H. Kimura, A. Inoue, *Appl. Phys. Lett.* **90** (2007) 241902-3
[11] S.P. Harimkar, S.R. Paital, A. Singh, R. Aalund, N.B. Dahotre, *J. Non-Cryst. Solids* **355** (2009) 2179-2182
[12] S. Lee, H. Kato, T. Kubota, A. Makino, A. Inoue, *Intermetallics* **17** (2009) 218-221
[13] H. Wang, Y. Liu, X. Pan, C. Feng, F. Ai, Y. Zhang, *J. Alloys Compds.* **477** (2009) 291-294
[14] S. Nowak, P. Ochin, A. Pasko, S. Guérin, Y. Champion, *Strength Mater.* **40** (2008) 154-157
[15] S. Nowak, P. Ochin, A. Pasko, O. Maciejak, P. Aubert, Y. Champion, *J. Alloys Compd.* **483** (2009) 139-142
[16] S. Nowak, L. Perrière, L. Dembinski, S. Tusseau-Nenez, Y. Champion, *J. Alloys Compd.* **509** (2011) 1011-1019
[17] M. Yamasaki, S. Kagao, Y. Kawamura, K. Yoshimura, *Appl. Phys. Lett.* **84** (2004) 4653-4655

https://doi.org/10.1051/metal/2011074 Published online by Cambridge University Press